Table 2. Translation of the Capitate and the Distal Fragment of the Scaphoid

			Capitate (mm)		
Type	Case	Duration (mo)	*x*	*y*	*z*
Proximal	1	8.6	1.18	−1.79	−0.76
Proximal	2	36.0	0.03	−0.56	0.16
Proximal	3	92.7	−0.95	−0.57	0.19
Proximal	4	97.0	−1.29	−2.09	1.12
Average		(Median: 64.4)	−0.26 mm	−1.25 mm	0.18 mm
Distal	5	3.0	−0.51	−2.04	−1.04
Distal	6	3.0	−0.35	−3.20	−0.09
Distal	7	3.1	1.46	−1.93	−1.67
Distal	8	5.6	−1.33	−2.53	−0.89
Distal	9	5.9	1.48	−1.78	0.22
Distal	10	7.1	−2.85	−2.86	0.07
Distal	11	8.9	0.49	−1.94	−0.43
Distal	12	13.4	−1.33	−5.54	−1.93
Distal	13	19.0	0.52	−2.48	−0.20
Distal	14	61.9	−0.72	−1.63	−0.48
Distal	15	111.0	−1.34	−4.35	−1.20
Distal	16	161.0	−2.99	−4.04	−2.00
Distal	17	192.0	−1.80	−3.02	0.12
Distal	18	240.0	−0.67	−3.25	−3.19
Distal	19	250.0	1.00	−6.43	−0.91
Distal	20	480.0	−1.13	−5.20	0.86
Average		(Median: 16.2)	−0.74 mm	−3.13 mm	−0.72 mm

tion was 3.2° ± 4.1°. For the lunate the mean extension was 5.4° ± 5.9° and the mean supination was 0.5° ± 2.7°. For the triquetrum the mean extension was 6.7° ± 6.2° and the mean supination was 1.3° ± 2.7°. Only 1 of the 4 patients with proximal fractures had DISI deformity. The rotations of the proximal fragment ($p < .01$) and the lunate ($p < .05$) to extension and supination were significantly smaller for proximal fractures than for distal fractures. There were no significant differences in the rotation of the triquetrum between proximal and distal fractures.

The capitate and the distal fragment translated in the dorsal direction 1.25 ± 0.80 mm and 0.77 ± 0.82 mm, respectively. The translation of the capitate and the distal fragment in the dorsal direction were sig-

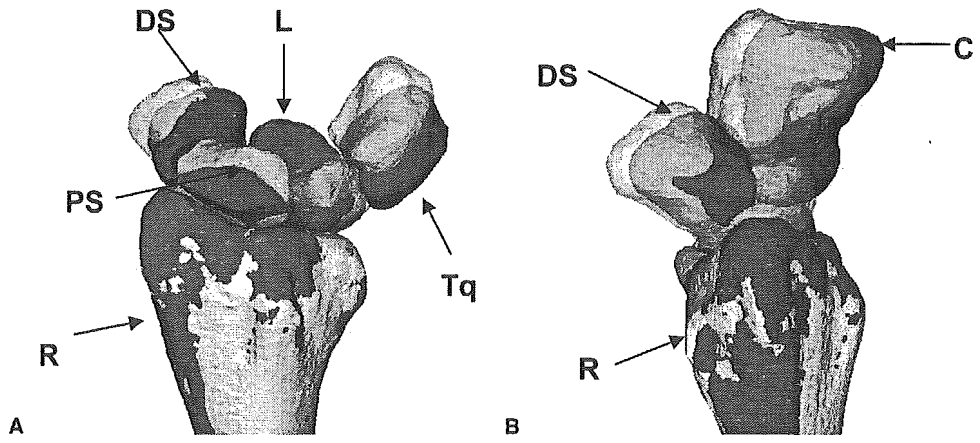

Figure 4. (A) Rotational displacement of the proximal row relative to the radius in distal fracture and (B) translation of the capitate and the distal fragment relative to the radius. The affected side (dark-colored parts) is superimposed on the contralateral uninjured side (gray-colored parts) on the basis of radius. R, radius; PS, proximal fragment of scaphoid; DS, distal fragment of scaphoid; L, lunate; Tq, triquetrum; C, capitate.

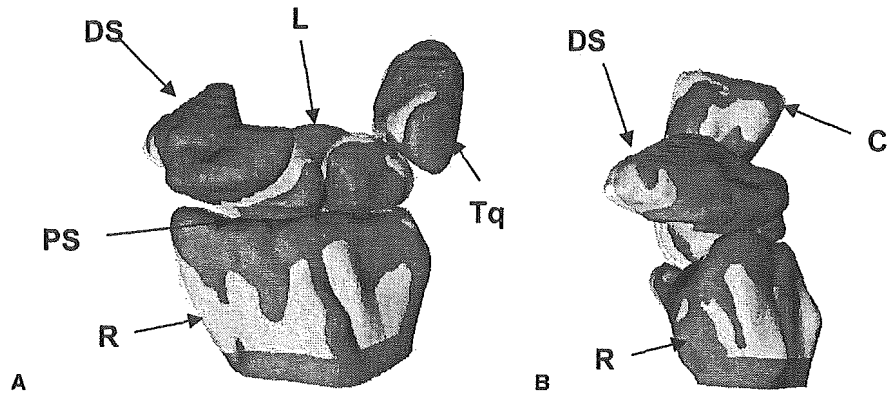

Figure 5. (A) Rotational displacement of the proximal row relative to the radius in proximal fracture and (B) translation of the capitate and the distal fragment relative to the radius. Displacements of the carpus are markedly small compared with distal fracture.

nificantly smaller for proximal fractures than for distal fractures ($p < .05$).

Discussion

Basic angulations and translation commonly were seen and recognized on standard tomography.[19] It is difficult, however, to characterize deformity of the carpus in scaphoid nonunion using 2-dimensional plain x-ray because of the complicated 3-dimensional structure and the overlapping of carpal bones in scaphoid nonunion. Three-dimensional analysis is essential for appropriate treatment of scaphoid nonunion with deformity. In the present study deformity of scaphoid nonunion and carpal collapse was quantified 3-dimensionally on the basis of the fracture location. For distal fractures the proximal fragment of the scaphoid and the lunate and triquetrum were extended and supinated and the capitate and the distal fragment translated in the dorsal direction without much rotation. A similar tendency regarding displacements was shown by proximal fractures but the degree of displacement was significantly smaller than for distal fractures.Under normal conditions with longitudinal load on the wrist the scaphoid tends to rotate into flexion and pronation along the articular surface of the trapezium and capitate and the triquetrum tends to rotate into extension and supination along the articular surface of the triquetrum–hamate joint.[20–22] These 2 opposing tendencies remain in equilibrium when the proximal row is stabilized (Fig. 6A).[23] If the DSLIL is torn the link with the proximal row is broken and the scaphoid rotates into flexion and pronation and the lunate and triquetrum rotate to extension and supination. With distal fractures this link is broken at the fracture site and the proximal row is no longer stabilized.[14,24] The proximal fragment linked to the lunate via the DSLIL rotates into extension and supination and the capitate and the distal fragment translate in the dorsal direction because of the extension effect of the lunate (Figs. 6B, C). Erosion of the palmar ulnar cortexes at the fracture site might proceed with the proximal fragment's extension and supination and result in humpback deformity. With proximal fractures this link survives and the proximal row remains stable (Fig. 6D). Moritomo et al[14] created a proximity map for scaphoid nonunions that was a visual representation of the distance between bones. Changes relative to this map are predictive of early degenerative changes. For distal fractures the proximity map location of the distal fragment is closer to the radial styloid compared with proximal fractures. Increased point loading and shear stresses on the articular cartilage beneath the abnormally positioned distal scaphoid fragment lead to degenerative changes at the radial styloid (Figs. 6C, 7A, B).[2,3,14,24–25] With proximal fractures the distal fragment remains linked to the lunate via the DSLIL so that the proximal row remains almost at equilibrium and the deformity is less marked than for distal fractures.[14,23] The capitate, however, might abut the fracture site and the proximal fragment, causing minor movement and resulting in late degenerative changes between the distal scaphoid and the dorsal position of the scaphoid fossa of the radius.[14,24]

In the present study the deformity of most of the carpus in scaphoid nonunion was analyzed and cases were classified into 2 patterns of deformity on the basis of fracture location. Regarding carpal deformity and subsequent degenerative change in scaphoid nonunion it appears that an important factor in the development of

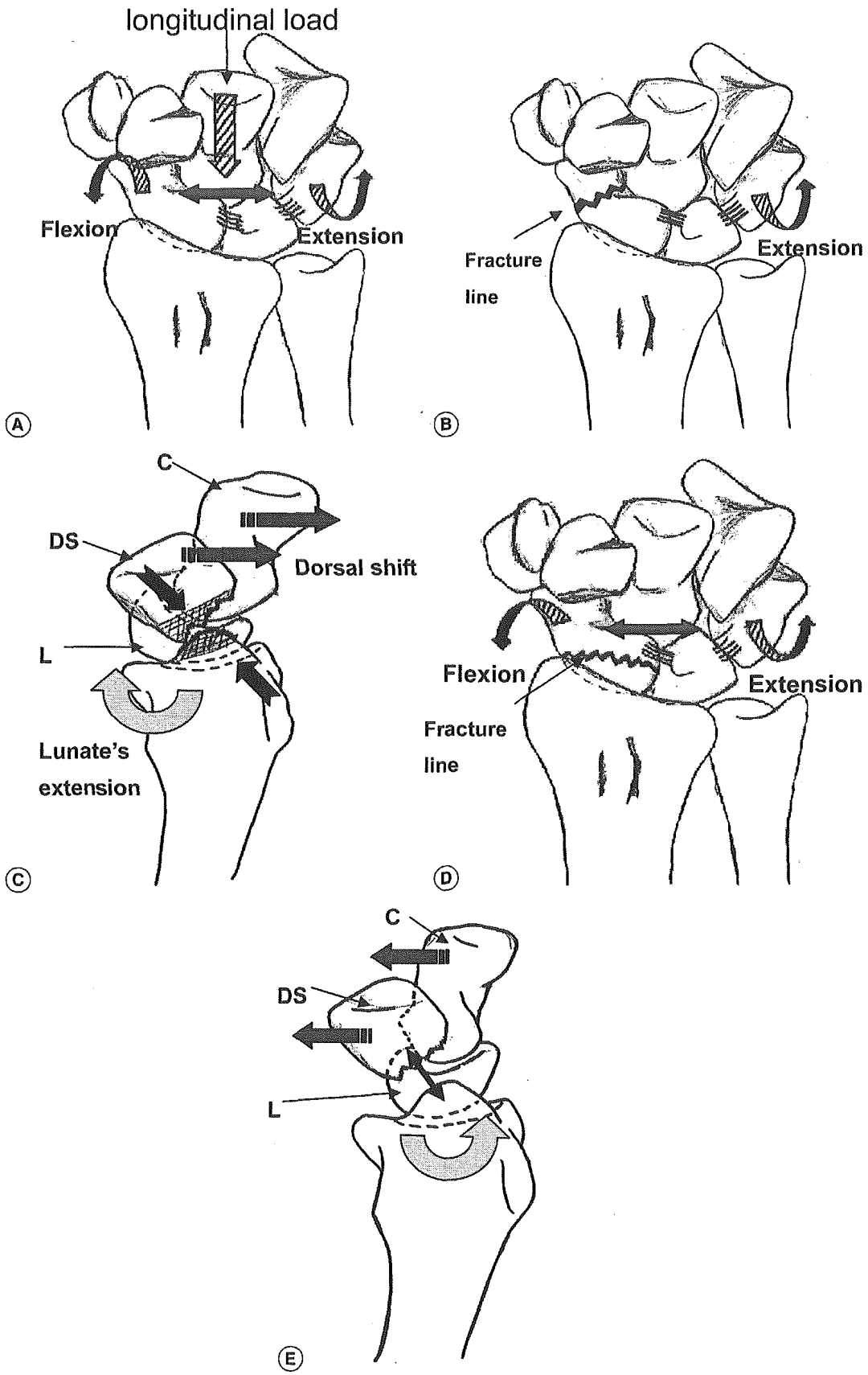

Figure 6. (A) Force of the scaphoid rotating into flexion and pronation counters the force of the triquetrum rotating into extension and supination. With distal fractures the link to the proximal row is broken at the fracture site. (B) The proximal fragment of the scaphoid and the lunate and triquetrum extend and supinate. (C) The capitate and the distal fragment translate in the dorsal direction because of the effect of the extension of the lunate. (D) With proximal fractures the link to the proximal row survives and the proximal row remains stable. (E) Correction of DISI deformity produces sufficient distance between the distal fragment and the radial styloid.

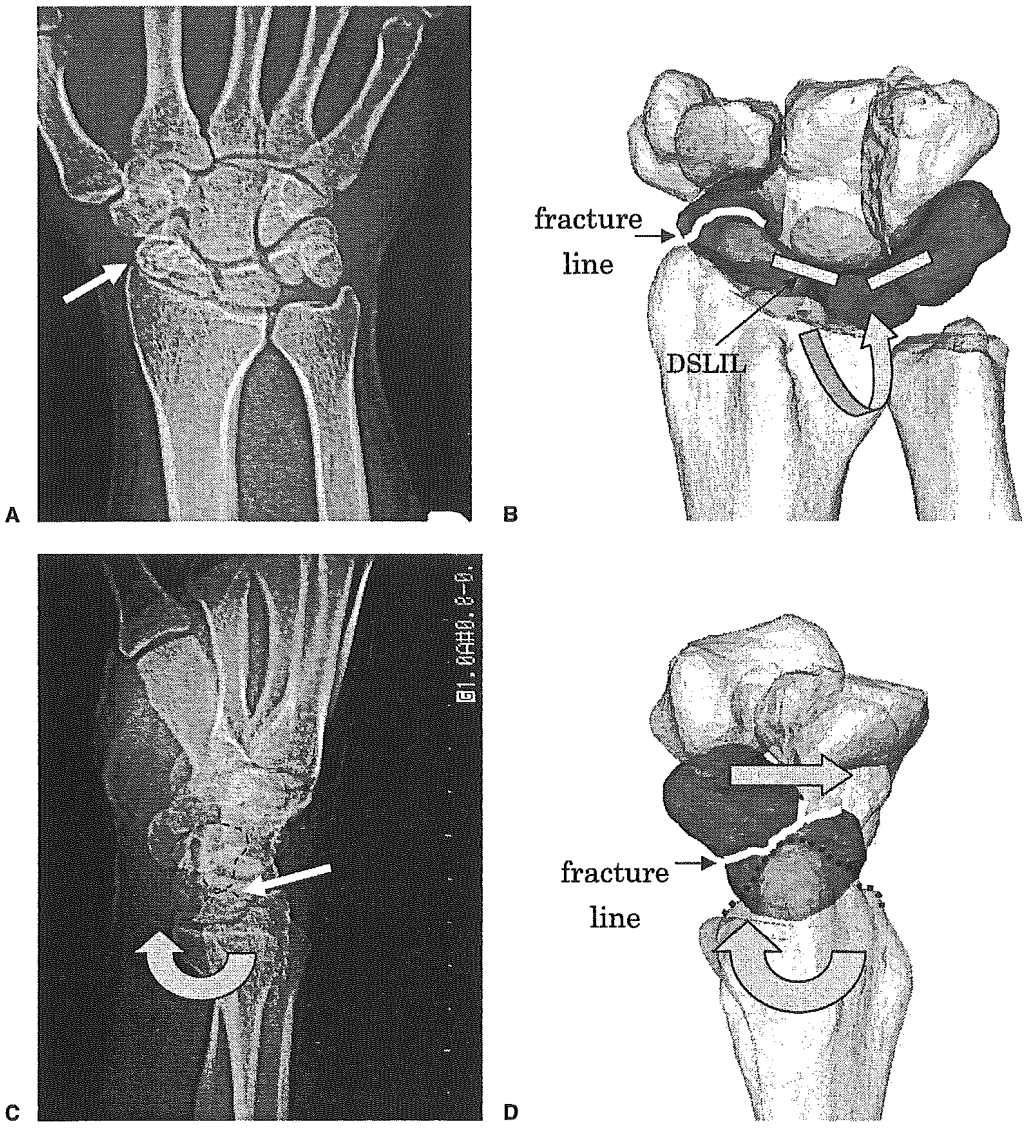

Figure 7. Anteroposterior view of (A) x-ray and (B) 3-dimensional surface model of scaphoid nonunion. The proximal fragment, lunate, and triquetrum rotated into extension and supination. Dogleg deformity of scaphoid nonunion and osteoarthritis of the radial styloid could be observed. (C) Lateral view of x-ray and (D) 3-dimensional surface model of scaphoid nonunion with osteoarthritis of the radial styloid. Extension of the proximal fragment and a dorsal shift of the distal fragment result in the humpback deformity in scaphoid nonunion.

this carpal deformity is whether the fracture line passes distal or proximal to the dorsoulnar apex of the scaphoid ridge and the DSLIL. With distal fractures the distal fragment translated dorsally, which might be one factor in the development of degenerative change at the radial styloid. Therefore we conclude that correction of DISI deformity is necessary for restoration of sufficient distance between the distal fragment and the styloid (Fig. 6E).The present study had some limitations. The number of proximal fracture nonunions (4 cases) was small compared with the distal fractures (16 cases). More cases of proximal fracture have to be investigated in the future to clarify the difference of the deformity between these 2 types. The second limitation was that the pattern of scaphoid fracture was more complicated than that classified in the present study. For instance, fractures of the tubercle (Herbert classification type A1) are very stable despite distal scaphoid fracture and comminuted fractures (Herbert classification type B5) are not included in this study. We believe, however, that considering the type of 3-dimensional information obtained in the present study in conjunction with the traditional classification such as the Herbert classification[26] can help surgeons characterize complex carpal deformity and the pathomechanism in scaphoid nonunion and that it can facilitate selection of appropriate treatment based on fracture location relative to the dorsal apex of the ridge.

The authors acknowledge the assistance during parts of the experimental procedure from Kouji Yamamoto, MD, from the Department of Orthopaedic Surgery, Toyonaka Municipal Hospital; Takeshi Yoshida, MD, from the Department of Orthopaedic Surgery, Kansai Rosai Hospital; Kazuhiro Masada, MD, from the Department of Orthopaedic Surgery, Osaka Rosai Hospital; and Ryoji Nakao, computer programmer, Department of Orthopaedic Surgery, Osaka University Graduate School of Medicine.

References

1. Fisk GR. Osteo-arthrosis of the wrist. Clin Rheum Dis 1984;10:571–588.
2. Mack GR, Bosse MJ, Gelberman RH, Yu E. The natural history of scaphoid non-union. J Bone Joint Surg 1984;66A: 504–509.
3. Ruby LK, Stinson J, Belsky MR. The natural history of scaphoid non-union. A review of fifty-five cases. J Bone Joint Surg 1985;67A:428–432.
4. Ruby LK, Leslie BM. Wrist arthritis associated with scaphoid nonunion. Hand Clin 1987;3:529–539.
5. Inoue G, Sakuma M. The natural history of scaphoid nonunion. Radiographical and clinical analysis in 102 cases. Arch Orthop Trauma Surg 1996;115:1–4.
6. Hidaka Y, Nakamura R. Progressive patterns of degenerative arthritis in scaphoid nonunion demonstrated by three-dimensional computed tomography. J Hand Surg 1998;23B:765–770.
7. Kozin SH. Incidence, mechanism, and natural history of scaphoid fractures. Hand Clin 2001;17:515–524.
8. Fisk GR. An overview of injuries of the wrist. Clin Orthop 1980;149:137–144.
9. Linscheid RL, Dobyns JH, Beckenbaugh RD, Cooney WP 3rd, Wood MB. Instability patterns of the wrist. J Hand Surg 1983;8:682–686.
10. Vender MI, Watson HK, Wiener BD, Black DM. Degenerative change in symptomatic scaphoid nonunion. J Hand Surg 1987;12A:514–519.
11. Kerluke L, McCabe SJ. Nonunion of the scaphoid: a critical analysis of recent natural history studies. J Hand Surg 1993; 18A:1–3.
12. Berdia S, Wolfe SW. Effects of scaphoid fractures on the biomechanics of the wrist. Hand Clin 2001;17:533–540.
13. Nakamura R, Imaeda T, Horii E, Miura T, Hayakawa N. Analysis of scaphoid fracture displacement by three-dimensional computed tomography. J Hand Surg 1991;16A:485–492.
14. Moritomo H, Viegas SF, Elder KW, Nakamura K, Dasilva MF, Boyd NL, Patterson RM. Scaphoid nonunions: a 3-dimensional analysis of patterns of deformity. J Hand Surg 2000;25A:520–528.
15. Lorensen W, Cline H. Marching cubes: a high resolution 3D surface construction algorithm. Computer Graphics 1987;21: 163–169.
16. Belsole RJ, Hilbelink DR, Llewellyn JA, Dale M, Greene TL, Rayhack JM. Computed analyses of the pathomechanics of scaphoid waist nonunions. J Hand Surg 1991;16A:899–906.
17. Besl PJ, Mackay N. A method for registration of 3-D shapes. IEEE Trans Patt Anal 1992;14:239–256.
18. Belsole RJ, Hilbelink DR, Llewellyn JA, Dale M, Ogden JA. Carpal orientation from computed reference axes. J Hand Surg 1991;16A:82–90.
19. Amadio PC, Berquist TH, Smith DK, Ilstrup DM, Cooney WP 3rd, Linscheid RL. Scaphoid malunion. J Hand Surg 1989;14A:679–687.
20. Weber ER. Biomechanical implications of scaphoid waist fractures. Clin Orthop 1980;149:83–89.
21. Kauer JM. Functional anatomy of the wrist. Clin Orthop 1980;149:9–20.
22. Smith DK, Cooney WP 3rd, An KN, Linscheid RL, Chao EY. The effects of simulated unstable scaphoid fractures on carpal motion. J Hand Surg 1989;14A:283–291.
23. Garcia-Elias M. Kinetic analysis of carpal stability during grip. Hand Clin 1997;13:151–158.
24. Garcia-Elias M, Lluch A. Partial excision of scaphoid: is it ever indicated? Hand Clin 2001;17:687–695.
25. Moritomo H, Tada K, Yoshida T, Masatomi T. The relationship between the site of nonunion of the scaphoid and scaphoid nonunion advanced collapse (SNAC). J Bone Joint Surg 1999;81B:871–876.
26. Herbert TJ, Fisher WE. Management of the fractured scaphoid using a new bone screw. J Bone Joint Surg 1984;66B: 114–123.

ELSEVIER

Journal of Orthopaedic Research 23 (2005) 750–756

Journal of Orthopaedic Research

www.elsevier.com/locate/orthres

In vivo three-dimensional wrist motion analysis using magnetic resonance imaging and volume-based registration

Akira Goto [a,b,*], Hisao Moritomo [b], Tsuyoshi Murase [b], Kunihiro Oka [b], Kazuomi Sugamoto [a], Takehiro Arimura [c], Jun Masumoto [d], Shinichi Tamura [d], Hideki Yoshikawa [b], Takahiro Ochi [a]

[a] *Division of Robotic Therapy, Osaka University Graduate School of Medicine, Japan*
[b] *Department of Orthopaedic Surgery, Osaka University Graduate School of Medicine, 2-2 Yamadaoka, Suita 565-0871, Japan*
[c] *Department of Radiology, Osaka University Hospital, Japan*
[d] *Division of Interdisciplinary Image Analysis, Osaka University Graduate School of Medicine, Japan*

Abstract

This study represents a new attempt to non-invasively analyze three-dimensional motions of the wrist in vivo. A volume-based registration method using magnetic resonance imaging (MRI) was developed to avoid radiation exposure. The primary aim was to evaluate the accuracy of volume-based registration and compare it with surface-based registration. The secondary aim was to evaluate contributions of the scaphoid and lunate to global wrist motion during flexion–extension motion (FEM), radio-ulnar deviation (RUD) and radial-extension/ulnoflexion, "dart-throwing" motion (DTM) in the right wrists of 12 healthy volunteers. Volume-based registration displayed a mean rotation error of 1.29° ± 1.03° and a mean translation error of 0.21 ± 0.25 mm and was significantly more accurate than surface-based registration in rotation. Different patterns of contribution of the scaphoid and lunate were identified for FEM, RUD, and DTM. The scaphoid contributes predominantly in the radiocarpal joint during FEM, in the midcarpal joint during RUD and almost equally between these joints during DTM. The lunate contributes almost equally in both joints during FEM and predominantly in the midcarpal joint during RUD and DTM.

Keywords: In vivo; Three-dimensional; Wrist kinematics; "Dart-throwing" motion; Volume-based registration

Introduction

Motion analysis has seen wide application in studies of normal and pathological kinematics and the effects of reconstructive procedures on pathological conditions. Researchers have recently been able to non-invasively measure three-dimensional (3D) in vivo kinematics of the wrist joint using 3D images [3,10]. These systems enable the viewing and analysis of any in vivo motion of one bone relative to another one with any joint motion. Current techniques utilize image registration to determine corresponding relations between several image volumes represented at different coordinates via computerized tomography (CT) [1]. As radiation exposure is unavoidable during the course of CT-based motion analyses, we have utilized magnetic resonance imaging (MRI) for image acquisition to develop non-invasive techniques [12].

Recent approaches in kinematic studies predominantly concentrated on surface-based registration [1,3]. A drawback of such methods is that registration

* Corresponding author. Address: Department of Orthopaedic Surgery, Osaka University Graduate School of Medicine, 2-2 Yamadaoka, Suita 565-0871, Japan. Tel.: +81 6 879 3552; fax: +81 6 879 3559.
E-mail address: goto-akira@umin.ac.jp (A. Goto).

0736-0266/$ - see front matter © 2004 Orthopaedic Research Society. Published by Elsevier Ltd. All rights reserved.
doi:10.1016/j.orthres.2004.10.001

accuracy is limited to the accuracy of the segmentation step of the images. More recently, volume-based registration methods have been developed and may have an advantage in that feature calculation is straightforward to the point that the accuracy of these methods is likely to be insensitive to segmentation errors [2]. A combination of MRI and volume-based registration may therefore afford accurate, non-invasive, in vivo, 3D kinematic studies of the wrist.

Several studies have examined how global wrist motion is apportioned among the radiocarpal and midcarpal joints [8]. Most previous kinematic studies, however, only investigated wrist flexion–extension motion (FEM) and radio-ulnar deviation (RUD). Wrist radial-extension/ulnoflexion motion, known as "dart-throwing" motion (DTM), has also been considered as one of the most essential human wrist motions [4,15]. Kinematics of this motion, however, has only been investigated a few times [6,18].

The primary aim of this study was to evaluate the accuracy of volume-based registration and compare it with that of surface-based registration. The secondary aim was to evaluate the contributions of the scaphoid and lunate to global wrist motion during wrist FEM, RUD, and, specifically, DTM.

Materials and methods

Comparison of accuracy between surface and volume-based registration

MRI data from the wrist joint of a fresh normal cadaver was obtained using a 1.5-T commercial MR system (Siemens: Magnetom Vision PlusR 1.5T MRI) in conjunction with a receive-only surface coil (CP flex large). We employed a 3D sequence (3dflash) with TR/TE of 2.3 ms/33 ms and flip angle of 45°, a 160 mm field of view and 0.5 mm thickness on contiguous slices, with pixels of 0.6×0.8 mm.

Segmentation is defined as extracting bone regions and associating each region with individual bones. The anatomical structure or region of interest needs to be delineated and separated so that it can be viewed individually and reconstructed as a 3D bone model. Regions of individual bones were semi-automatically segmented from MR volume images using the Virtual Place-M® software developed in our laboratory (Medical Imaging Laboratory, Tokyo, Japan). This software generates 3D surface bone models by gathering pieces from all the slices, using the Marching Cubes technique [9]. From this software, we obtained surface models of each carpal bone, the ulna, and the radius without the cartilage using a Precision 650 DELL graphics workstation 3.20 GHz Pentium4 Xeno Dual Processor, 4 GB RAM.

Surfaced-based registration was performed using independent implementation of the interative closest point registration algorithm of Besl and McKay [1]. The method involves a two-step process. First, the closest point on one surface is computed for each point in a set of points representing the other surface. In this study, the first surface was a triangle set representation of the bone surface in the MR image, and the point set representation of the second surface was a set of surface points extracted from the other position image. Second, a transformation is determined by registering these two point sets. This process is iterated until some terminating criterion is satisfied. This method converges to a local minimum of the cost function, which is the root mean square (rms) distance between corresponding points at the final iteration.

Volume-based registration represents a method for determining relative positions between volume images represented at different coordinates, which means overlapping voxels in the intersection region of the baseline (target) and transformed images using a corresponding method based on correlation between voxel values. This overlapped region X_0 is set as the subset of voxel N_0 locations of the baseline image and $X_0 = \{X_0 : X_0 \in X \cap T(X')\}$ where T is the rigid body transformation. The intensity of a voxel located at X_0 in the baseline image is denoted by $f(X_0)$, and the corresponding one in the transformed image by $g(X_0)$. The sets of intensities of the overlapping voxels of the baseline and transformed images are referred to as $F(X_0)$ and $G(X_0)$.

The normalized correlation coefficient (NCC) was used as a measure of similarity. Using this method, each carpal bone in one position was superimposed over images for each position. Relative motion of the carpal bones were then calculated by starting from initial translation parameters and finally finding the parameters allowing maximal correlation of the two images [2]. We sought the maximal NCC(F, G):

$$\mathrm{NCC}(F,G) = \frac{1}{N_0^2} \frac{\sum_{x_0 \in X_0} (f(x_0) - \bar{f})(g(x_0) - \bar{g})}{\sigma_f \sigma_g}$$

where $\bar{f}$ and $\bar{g}$ are the mean intensities of $F(X_0)$ and $G(X_0)$ and

$$\sigma_f = \frac{1}{N_0} \sqrt{\sum_{x_0 \in X_0} (f(X_0) - \bar{f})^2}, \quad \sigma_r = \frac{1}{N_0} \sqrt{\sum_{x_0 \in X_0} (g(X_0) - \bar{g})^2}$$

The experiment was conducted to determine and compare the accuracy from the two registration methods. Accuracies were evaluated using gold standards that were based on the parameters of the centroid position of fiducial markers. Fiducial markers were spheres of 7 mm diameter with oil inside that showed as hyperintense silhouettes on MRI. Markers were attached to the cadaver during image acquisition. The cadaver was scanned 10 times from different directions randomly using 3D-MRI. The position of a marker was defined by its centroid. An intensity-based centroid was calculated for each marker using the localization technique described in Wang et al. [16]. Validations of each registration were based on this transformation parameter of centroids. Ten registrations were examined in 10 MR images.

Motion analysis

Contributions of the scaphoid and lunate to global wrist motion were studied during wrist FEM, RUD, and DTM using MRI and volume-based registration techniques. The right wrists of 12 healthy volunteers (4 women and 8 men; age range 20–34 years, mean age 26.1 years) were studied. Each volunteer was positioned in the magnet in a lateral recumbent position with the elbow in 90° flexion during MR acquisition. Informed consent was obtained from each person according to institutional review board protocol.

For a global contribution study, images were obtained in three positions during wrist FEM, RUD, and DTM (a neutral position and the two extreme positions of each motion). Incremental contributions of the scaphoid and lunate were investigated during wrist FEM, RUD and DTM in five subjects. For the incremental contribution study, images were obtained in seven positions of FEM (60°, 40°, 20°, and 0° of flexion and 20°, 40°, and 60° of extension), RUD (radial deviation to 20°, 10°, and 0° and ulnar deviation to 10°, 20°, 30°, and 40°), and DTM (radial extension to extreme position and ulnar flexion to extreme position).

Accurate 3D visualization and estimates of relative positions and orientations of the capitate, scaphoid, and lunate relative to the radius were obtained using registration techniques and Euler angles. Euler angles represent the description of angular motions of a body in 3D space. Wrist motion was expressed as a ratio of radius/lunate or radius/scaphoid motion relative to radius/capitate motion. In-plane angles (sagittal plane corresponding to FEM, coronal plane to RUD, and oblique plane to DTM) of the radius/scaphoid, radius/lunate, and radius/capitate were measured directly from motion analysis data. The midcarpal joint (scaphoid/capitate, lunate/capitate) angle was calculated as the radius/capitate angle minus the radiocarpal (radius/scaphoid, radius/lunate) joint angle.

In studies of FEM and RUD, the coordinate system was constructed using ISB (based on the International Society of Biomechanics proposed standard definition for the wrist joint: http://www.

isbweb.org/standards/wrist.html). The origin is located between the radioscaphoid fossa and the radiolunate fossa. The *Y*-axis was defined as the line parallel to the long shaft of the radius with the long shaft axis corresponding to the minimum moment of inertia. The *Z*-axis was perpendicular to the *Y*-axis in a plane defined by the tip of the radial styloid, the base of the concavity of the sigmoid notch, and the specified origin. The *X*-axis was perpendicular to the *Y* and *Z* axes.

In the study of DTM, the dart-throwing plane was separately calculated for each subject and was defined as a plane that included the origin of the coordinate system and two centroids of the volume of the capitate at wrist extreme radial-extension and extreme ulnoflexion. Contributions of the scaphoid and lunate to global wrist motion during DTM were evaluated by calculating projection angles of each carpal bone to the dart-throwing plane. The calculated dart-throwing plane deviated 22.9° ± 8.8° ulnarly and pronated 17.2° ± 10.8° relative to the sagittal plane of the wrist in average.

Results

Comparison of accuracy between surface- and volume-based registration

Volume-based registration showed a mean rotation error of 1.29° ± 1.03° and a mean translation error of 0.21 ± 0.25 mm (Table 1). Surface-based registration had a mean rotation error of 1.67° ± 0.90° and a mean translation error of 0.19 ± 0.14 mm. Volume-based registration was more accurate in terms of rotation error ($p < 0.05$, two-tailed paired *t*-test). No significant difference in the translation components were noted between the two methods ($p = 0.503$).

Motion analysis

Different patterns of orientations relative to the radius of the capitate, scaphoid, and lunate were noted for FEM, RUD, and DTM (Figs. 1 and 2). The scaphoid contributed predominantly in the radiocarpal joint during FEM ($p < 0.001$), in the midcarpal joint during RUD ($p < 0.005$), and almost equally to both joints during DTM (Table 2). The lunate contributed almost equally in both joints during FEM and predominantly in the midcarpal joint during both RUD and DTM ($p < 0.05$, *t*-tests).

Table 1
Accuracy of surface- and volume-based registration for each carpal bone

	Carpal bone						
	Capitate	Hamate	Lunate	Scaphoid	Trapezium	Trapezoid	Triquetrum
Accuracy of surface-based registration							
Rotation error	1.70 (0.55)	1.26 (0.67)	1.91 (0.78)	1.36 (0.67)	1.38 (0.78)	2.20 (1.11)	1.87 (0.91)
Translation error	0.14 (0.09)	0.17 (0.17)	0.13 (0.14)	0.16 (0.08)	0.23 (0.13)	0.24 (0.19)	0.19 (0.11)
Accuracy of volume-based registration							
Rotation error	1.17 (1.01)	1.01 (0.76)	1.28 (0.72)	0.69 (0.35)	1.37 (1.55)	2.08 (1.64)	1.40 (0.79)
Translation error	0.12 (0.17)	0.23 (0.31)	0.14 (0.13)	0.17 (0.23)	0.32 (0.42)	0.37 (0.28)	0.24 (0.26)

An average of rotation and translation errors for each bone was measured. Rotation error unit: degree (standard deviation), translation error unit: millimeter (standard deviation).

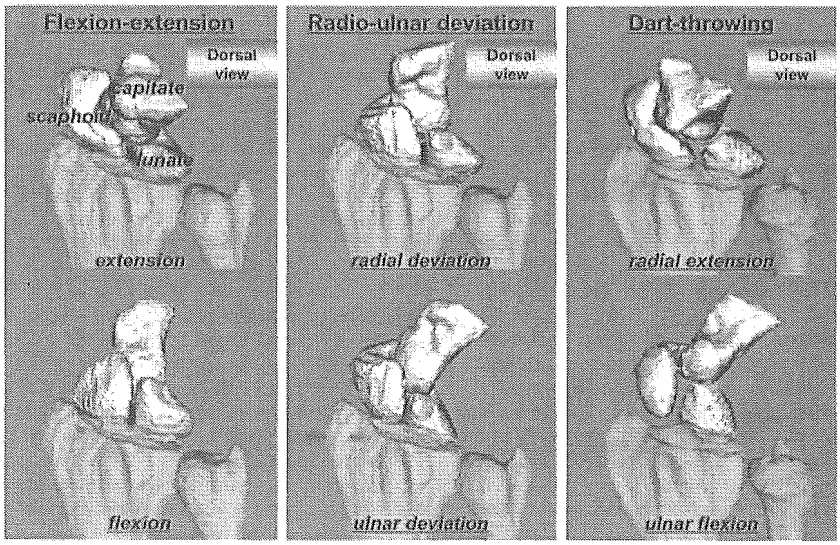

Fig. 1. Three-dimensional motion of the scaphoid, lunate, and capitate relative to the radius during flexion–extension (FEM), radio-ulnar deviation (RUD), and dart-throwing motion (DTM). In the dorsal view, each carpal bone moves in a different pattern. A part of the dorsal rim of the distal radius has been made translucent so that the proximal scaphoid and lunate can be seen clearly.

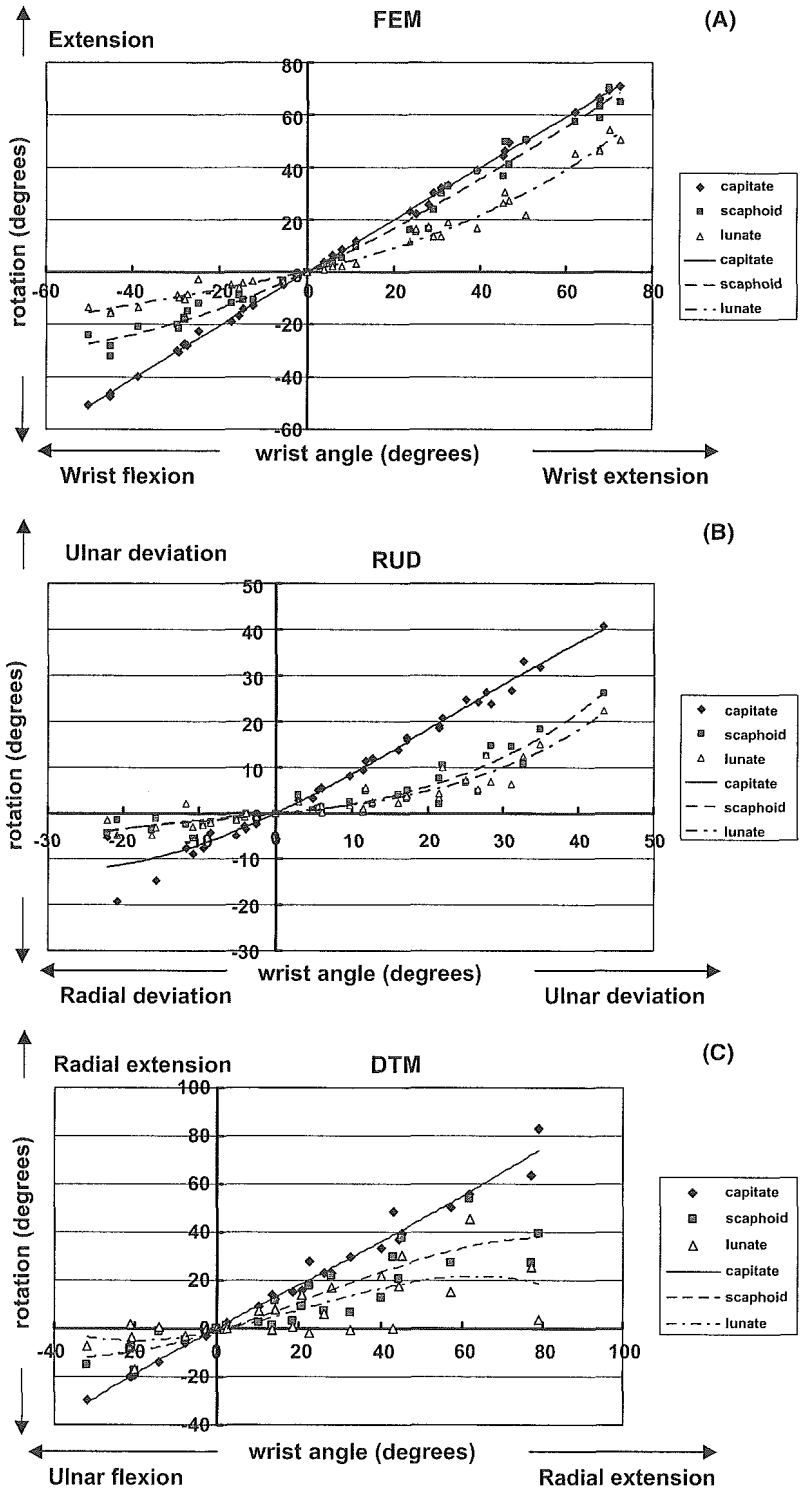

Fig. 2. Incremental contribution study of the capitate, scaphoid, and lunate: (A) flexion–extension motion, (B) radio-ulnar deviation, (C) dart-throwing motion. The vertical axis shows the rotation angle of carpal bones in-plane (in the case of FEM in-plane becomes the sagittal plane, but becomes the coronal plane during RUD and the oblique plane during DTM). The horizontal axis shows the angle of wrist position. The angle of wrist position is defined as the rotation angle of radiocapitate.

We found relatively great motion of the scaphoid despite of small motion of the lunate during DTM. In wrist radial-extension the scaphoid contributed 49.3% of capitate motion, and the lunate contributed only 21.7% in the radiocarpal joint. In wrist ulnoflexion, the scaphoid contributed 50.6%, and the lunate contributed only 31.1% in the radiocarpal joint. The ratio of scaphoid motion to lunate motion in the radiocarpal

Table 2
Global contribution of the scaphoid and lunate rotation to the radiocapitate rotation during flexion–extension (FEM), radio-ulnar deviation (RUD), and dart-throwing motion (DTM) for 12 subjects

Joint	Motion	Scaphoid				Lunate			
		Rotation (°)	SD (°)	Contribution (%)	AV (%)	Rotation (°)	SD (°)	Contribution (%)	AV (%)
FEM									
Radiocarpal	Ext.	52.0	8.5	88.9	81.7	38.8	10.8	63.4	56.4
	Flex.	23.5	6.1	69.7		13.9	5.7	43.2	
Midcarpal	Ext.	6.7	7.5	11.1	18.3	22.4	16.2	36.6	43.6
	Flex.	10.2	7.1	30.3		18.3	9.8	55.8	
RUD									
Radiocarpal	Radial dev.	3.4	2.0	24.8	36.0	3.3	2.7	28.0	36.8
	Ulnar dev.	12.8	5.8	40.9		12.6	5.6	40.1	
Midcarpal	Radial dev.	10.3	7.3	75.2	64.0	8.5	10.3	72.0	63.2
	Ulnar dev.	18.5	4.8	59.1		18.8	3.8	59.9	
DTM									
Radiocarpal	Radial ext.	27.1	12.1	49.3	49.6	12.0	7.5	21.7	26.4
	Ulnar flex.	7.8	5.9	50.6		3.3	6.1	31.1	
Midcarpal	Radial ext.	27.8	12.2	50.7	50.4	43.3	20.2	78.3	73.6
	Ulnar flex.	7.6	5.5	49.4		7.3	16.1	68.9	

Average rotation angle was measured from neutral wrist position to each extreme position. SD = standard deviation, AV = a contribution ratio of the scaphoid and lunate in the each carpal joint.

joint was 1.43 during FEM, 1.02 during RUD, and 2.28 during DTM. These results indicate scaphoid motion relative to lunate motion in the radiocarpal joint is greater during DTM than FEM and RUD.

During FEM, the scaphoid ($r^2 = 0.99$) moved in a ratio of 1:2 (midcarpal:radiocarpal joint) from full flexion to neutral wrist position, but from neutral to full extension, mainly moved in the radiocarpal joint. During RUD, the scaphoid ($r^2 = 0.91$) moved almost linearly and predominantly acted in the midcarpal joint from full radial deviation to 10° of ulnar deviation. But from 10° of ulnar deviation to full ulnar deviation, the ratio of midcarpal to radiocarpal joint gradually increased, and at the end the ratio became almost 2:3. During DTM, the scaphoid ($r^2 = 0.89$) moved almost linearly and with almost the same contribution ratio in the radiocarpal and midcarpal joints (Fig. 2).

During FEM, the lunate ($r^2 = 0.98$) moved in an almost linear manner in both the radiocarpal and midcarpal joints from full flexion to 30° of wrist extension, then the ratio of midcarpal to radiocarpal joint gradually increased and predominantly acted in the radiocarpal joint. During RUD, the lunate ($r^2 = 0.90$) moved with almost the same pattern as the scaphoid. During dart-throwing motion, the lunate ($r^2 = 0.55$) moved with almost the same contribution ratio in the radiocarpal and midcarpal joints from 10° of ulnar flexion to 40° of radial extension, but nearly plateaued or decreased on other degrees.

Discussion

This study represents a new attempt to analyze 3D motions of the wrist in vivo in a non-invasive manner. MRI was used for image acquisition to avoid radiation exposure, which has been unavoidable in previous CT-based motion analyses. Our technique can be more beneficial than CT-based analysis in clinical situations for obtaining information such as preoperative pathological kinematics of the patient and outcomes of surgical procedures in reconstructive surgery.

The volume-based registration method is based on matching of bony contour and content data in all images by similarity of the image intensity. The accuracy of this method is likely to be less sensitive to segmentation errors than surface-based registration. West et al. performed a comparative study of surface- and volume-based registrations between intermodality images of the human brain [19]. They concluded that volume-based registration tends to be more accurate than surface-based registration. Moojen et al. reported that their volume method is more accurate than a surface method in CT-based registration [11]. In a wrist kinematic study, Neu et al. reported the accuracy of 3D surface registration [14]. Rotation errors for the capitate and scaphoid were less than 0.5°, for the other bones were generally less than 2°, and for trapezoid was greater than 2°. Translation errors for the bones were generally less than 1 mm, except for the trapezoid. Our accuracy rates were similar, especially for the trapezoid, with rates for both

around 2°. The poor accuracy for the trapezoid may be because of the shape of the bone. Our results correlate well with those studies, and subvoxel accuracy can be achieved, making this method very well suited to clinical applications and research.

Our data regarding global contributions during FEM and RUD largely concurred with data presented in the literature. However, the incremental contributions to wrist motion have been reported in only a few studies, and most investigations utilized in vitro studies. Recently, Crisco and colleagues reported incremental wrist motion from in vivo CT-based kinematic studies [4,20]. They concluded that scaphoid and lunate contributions to global wrist flexion changed in a linear manner with each wrist position. In our results, during DTM in vivo 3D incremental contributions changed in a linear manner, but during FEM and RUD, were not constant and changed at each wrist position, particularly for scaphoid motion.

Wrist motion in the oblique plane from radial-extension to ulnoflexion is used in many activities in daily life, such as hammering nails or throwing objects [5], and this oblique plane is believed to involve more mobility and agility [6,15]. However, kinematics of this motion data have rarely been reported, and all previous research has utilized two-dimensional or in vitro studies. Saffar and Semaan stated that a significant part of the movement takes place in the midcarpal joint during DTM, and movement in the midcarpal joint is oblique [15]. Ishikawa et al. reported that more motion of the scaphoid and lunate in the midcarpal joint was observed during DTM than during FEM [7]. Werner et al. suggested that there may be a dart throw motion during which there may be minimal scaphoid and lunate motion [17].

While our results support these conclusions in terms of the lunate (contribution of the lunate at the midcarpal joint during DTM was 80.2% in radial-extension and 77.3% in ulnoflexion), the scaphoid was found to contribute almost equally in both radiocarpal and midcarpal joints during DTM. First, these differences may be caused by differences in the plane of DTM between in vitro and in vivo. Ishikawa et al. defined the plane of DTM as at an angle of 23° to the sagittal plane. In contrast, the dart-throwing plane calculated in our study was more complex, being more functional and physiological, deviating 22.9° ± 8.8° ulnarly and pronating 17.2° ± 10.8° relative to the sagittal plane. Second, we think that dart throw motion consists of moving a combination of carpal and distal raidounlar joint. There was a tendency of the forearm being in a slightly pronated position during dart throw motion. Therefore, the movement of the scaphoid in the radiocarpal joint increased (49.6% of wrist motion). Saffar and Semaan suggested that the scaphoid displays more significant excursion in extension, sliding dorsal to the radial styloid in the dart-throwing plane. Moritomo et al. reported that the scaphotrapezio-trapezoid joint displays strong ligamentous and skeletal constraints, and therefore the direction of motion is limited to an almost 45° oblique plane relative to the sagittal plane [12,13]. We speculate that scaphoid motion in the midcarpal joint is constrained more than lunate motion, and the radioscaphoid and scapholunate joints must therefore move effectively to achieve congruent motion of the carpal bones during DTM.

Acknowledgments

The authors wish to acknowledge the invaluable contributions to the experimental procedure from: Yoshikazu Nakajima, PhD, of the Department of Medical Robotics and Image Sciences, Osaka University Graduates School of Medicine; Takehiro Arimura, RT, from the Department of Radiology, Osaka University Graduates School of Medicine; and Ryoji Nakao (MMT Co.).

References

[1] Besl PJ, Mackay N. A method for registration of 3-D shapes. IEEE Trans Pattern Anal 1992;18(14):239–56.
[2] Brown LG. A survey of image registration techniques. ACM Comput Surveys 1992;24(4):325–76.
[3] Crisco JJ, McGovern RD, Wolfe SW. Three-dimensional joint kinematics using bone surface registration: a computer assisted approach with an application to the wrist joint in vivo. MICCAI 1998:696–9.
[4] Crisco JJ, Wolfe SW, Neu CP, Pike S. Advances in the in vivo measurement of normal and abnormal carpal kinematics. Orthop Clin North Am 2001;32(2):219–31, vii.
[5] Fisk GR. Biomechanics of the wrist joint. In: The Hand. Philadelphia: WB Saunders; 1981.
[6] Garcia-Elias M. Carpal instabilities and dislocations. In: Green's operative hand surgery. 4th ed. Philadelphia: Churchill Livingstone; 1999.
[7] Ishikawa J, Cooney 3rd WP, Niebur G, et al. The effects of wrist distraction on carpal kinematics. J Hand Surg [Am] 1999; 24(1): 113–20.
[8] Kobayashi M, Berger RA, Linscheid RL, An KN. Intercarpal kinematics during wrist motion. Hand Clin 1997;13(1):143–9.
[9] Lorensen W, Cline H. Marching cubes: a high resolution 3D surface construction algorithm. Comput Graphics 1987;21:163–9.
[10] Moojen TM, Snel JG, Ritt MJ, et al. Three-dimensional carpal kinematics in vivo. Clin Biomech (Bristol, Avon) 2002;17(7): 506–14.
[11] Moojen TM, Snel JG, Ritt MJ, et al. In vivo analysis of carpal kinematics and comparative review of the literature. J Hand Surg [Am] 2003;28(1):81–7.
[12] Moritomo H, Goto A, Sato Y, et al. The Triquetrum-hamate joint: an anatomic and in vivo three-dimensional kinematic study. J Hand Surg [Am] 2003;28(5):797–805.
[13] Moritomo H, Viegas SF, Elder K, et al. The scaphotrapeziotrapezoidal joint. Part 2: a kinematic study. J Hand Surg [Am] 2000;25(5):911–20.
[14] Neu CP, McGovern RD, Crisco JJ. Kinematic accuracy of three surface registration methods in a three-dimensional wrist bone study. J Biomech Eng 2000;122(5):528–33.
[15] Saffar P, Semaan I. The study of the biomechanics of wrist movements in an oblique plane. In: Advances in the biomechanics

of the hand and wrist. 11th ed. New York: Plenum Press. p. 305–11.
[16] Wang MY, Maurer Jr CR, Fitzpatrick JM, Maciunas RJ. An automatic technique for finding and localizing externally attached markers in CT and MR volume images of the head. IEEE Trans Biomed Eng 1996;43(June):627–37.
[17] Werner FW, Green JK, Short WH, Masaoka S. Scaphoid and lunate motion during a wrist dart throw motion. J Hand Surg [Am] 2004;29(3):418–22.
[18] Werner FW, Palmer AK, Somerset JH, et al. Wrist joint motion simulator. J Orthop Res 1996;14(4):639–46.
[19] West JB, Fitzpatrick JM, Wang MY, et al. Retrospective intermodality registration techniques for images of the head: surface-based versus volume-based. IEEE Trans Med Imaging 1999;18:144–50.
[20] Wolfe SW, Neu C, Crisco JJ. In vivo scaphoid, lunate, and capitate kinematics in flexion and in extension. J Hand Surg [Am] 2000;25(5):860–9.

CLINICAL ORTHOPAEDICS AND RELATED RESEARCH
Number 434, pp. 143–150

Does Three-dimensional Computer Simulation Improve Results of Scaphoid Nonunion Surgery?

Tsuyoshi Murase, MD, PhD; Hisao Moritomo, MD, PhD; Akira Goto, MD; Kazuomi Sugamoto, MD, PhD; and Hideki Yoshikawa, MD, PhD

The purpose of this study was to clarify the effectiveness of the three-dimensional computer simulations in scaphoid nonunion surgery. Seven consecutive clinical patients with scaphoid nonunion at the middle third comprised the study group. Surface models of the scaphoid were constructed on the computer using computed tomography data of the bilateral wrists in neutral position. The distal and proximal fragments of the nonunion model were matched to the mirror image of the contralateral scaphoid model. The rotation of the distal fragment relative to the proximal fragment was calculated, and reduction of the displaced fragment of the scaphoid nonunion was simulated. Similarly, the estimated bone defect and the appropriate site and direction of the screw insertion were simulated. Full-sized hard models of the bone, including a model with simulated reduction and screw insertion, then were made using stereolithography based on the computer data. In the actual surgery, reduction, bone grafting, and screw insertion were achieved using the hard models as guides. All the patients obtained solid bone fusion and substantial clinical improvement with normalized scapholunate and radiolunate angles after surgery. Three-dimensional computer simulations were found as useful for accurate correction of scaphoid nonunions and proper screw placement, which consequently leads to good clinical results.

In scaphoid nonunions, the distal fragments usually rotate volarly, whereas the proximal fragments rotate dorsally, resulting in a humpback deformity with an evident dorsal intercalated segment instability (DISI) pattern of the carpal bones.[32] If the deformity is left untreated, osteoarthritis progresses initially at the radioscaphoid articulation, eventually affecting the midcarpal joint.[9,20,26,36] Incongruence of the joint surfaces and loss of carpal stability resulting from the displaced scaphoid nonunion are considered the major factors of these progressive degenerative changes.[26] Anterior wedge-shaped bone grafting has been advocated since the 1970s to correct carpal malalignment, restore normal scaphoid anatomy, and potentially avoid degenerative complications.[9,11–13,15,28,34,35] However, there has been no standard method to simulate the precise correction of this three dimensionally complex deformity.

Another problem of scaphoid nonunion surgery is the difficulty of screw insertion. Proper orientation and insertion of a screw across the ununited scaphoid may be technically difficult. The jig is not always positioned accurately to the bone. Improper placement of the screw results in loss of fixation and could be a critical cause of nonunion after anterior wedge-shaped bone grafting and screw insertion.[9]

However, during the last decade the continued developments in computed tomography (CT) hardware and computer technology have enabled simulated orthopaedic surgery with three-dimensional (3-D) models.[16,33] Since 2001, we have attempted to simulate the surgery for scaphoid nonunion using 3-D models from CT data to achieve three dimensionally accurate reductions and correct screw insertion. We wished to determine whether the 3-D computer simulation of the scaphoid nonunion helps us to reduce the displaced fragments correctly, insert the screw in the appropriate position, and as a result improve the radiographic and clinical results after the surgery?

MATERIALS AND METHODS

Seven consecutive patients with scaphoid nonunion (Table 1) comprised the study group. Inclusion criteria were nonunion at the middle third, surgery done more than 3 months after the

Received: June 3, 2004
Revised: September 27, 2004
Accepted: December 6, 2004
From the Department of Orthopaedic Surgery, Osaka University Graduate School of Medicine, Osaka, Japan.
Tsuyoshi Murase, MD, PhD received funding from NEDO (New Energy and Industrial Technology Development Organization) of Japan.
Each author certifies that his or her institution has approved the human protocol for this investigation and that all investigations were conducted in conformity with ethical principles of research, and that informed consent was obtained.
Correspondence to: Tsuyoshi Murase, MD, PhD, Department of Orthopaedic Surgery, Osaka University Graduate School of Medicine, 2-2, Yamada-oka, Suita, Osaka 565-0871, Japan. Phone: 81-6-6879-3552; Fax: 81-6-6879-3559; E-mail: murase-t@umin.ac.jp.

TABLE 1. Patient Data

Patient Number	Age at Surgery (years)	Gender	Affected Side	Duration of Nonunion (months)	Followup (months)
1	22.1	F	R	9	15.6
2	20.2	M	L	3	15.4
3	18.2	M	R	6	12.1
4	21.9	M	L	13	13.1
5	42.4	M	L	62	15.7
6	18.4	M	L	3	12.5
7	24.2	M	L	18	15.1

initial injury, and age older than 18 years. Exclusion criteria were proximal or distal pole nonunion, fresh fracture, age younger than 17 years, and preoperative osteoarthritic change seen on plain radiographs. Six patients were men and one patient was a woman. The right wrist was affected in two patients, and the left wrist was affected in five patients. The time between injury and surgery averaged 12.6 months (range, 3–36 months). Four patients had received no treatment for the original fracture, two patients had been misdiagnosed, and one patient had chosen to discontinue the initial treatment. All patients had moderate wrist pain when using the affected hand. Patients were an average of 23.9 years (range, 18–42 years) at the time of surgery. They then were followed up for more than 12 months.

Computed tomography scans of the bilateral wrists with a slice thickness of 0.625 mm and pixel size of 0.625×0.625 mm were taken (General Electrics, High Speed Advance or LightSpeed Ultra 16, Waukesha, WI) with the patient in the prone position with the arms elevated over the head. Data were saved as Digital Imaging and Communications in Medicine (DICOM) format. To maintain the wrists in neutral position, splints made of radiolucent material were worn during image acquisition. The contour of the scaphoid bone was semiautomatically segmented using commercially available software (Virtual Place M®, Medical Imaging Laboratory, Tokyo, Japan), and a surface model of the bone was constructed by applying a 3-D surface generation of the bone's cortex using the marching cubes algorithm.[24] The geometric models of the scaphoid bone were observed using this computer program (Fig 1).

Using the graphic work station, the distal and proximal fragments of the nonunion model were matched to the mirror image of the contralateral scaphoid model using iterative closest point (ICP) algorithm, which is one of the most advanced methods for surface-based registration.[3] In this method, a 3-D surface model and a set of 3-D points are registered starting from initial transformation parameters and finally finding the best parameters, while minimizing the sum of the distance from each 3-D point to the surface. The proximal and distal fragments of the nonunion model were registered with the proximal and distal parts of the mirror image of the contralateral normal scaphoid, respectively. Therefore, the rotation of the distal fragments relative to the proximal fragment were calculated using a screw displacement axis system.[22] In this way, we simulated reduction of the displaced fragments of the scaphoid nonunion (Fig 2A).

The estimated bone defect was calculated by subtracting the reduced nonunion model from the mirror image of the contralateral normal scaphoid by means of Boolean operation using the commercially available computer software (Magics RP®, Materialise, Leuven, Belgium). The appropriate site and direction of the screw insertion were similarly simulated by observing the model transparently or observing the transverse section of the reduced nonunion models after trial insertion of the screw on the computer monitor (Fig 2B). The screw was simulated to be placed along the longitudinal axis of the scaphoid and into the center of the proximal fragment. The estimated longest length of the screw was defined as the distance between the volar and dorsal cortex of the scaphoid where the simulated screw insertion pierces.

To facilitate the reproduction of computer simulations in the actual operation, full-sized stereolithography models (hard mod-

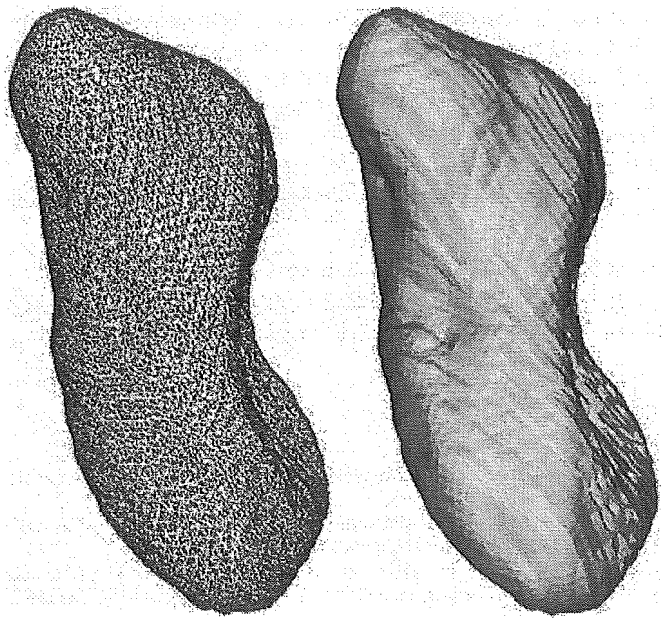

Fig 1. A 3-D surface model of the scaphoid as reconstructed by computer shows the frame model (right) and surface model (left).

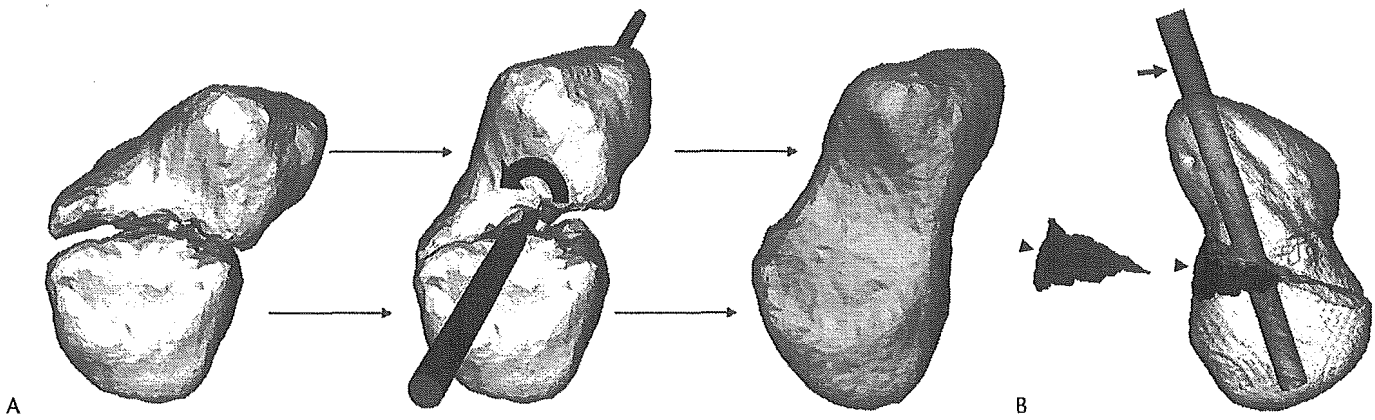

Fig 2A–B. (A) To simulate reduction of the displaced scaphoid, the distal and proximal fragments of the nonunion model (left) were registered to the mirror image of the contralateral normal scaphoid model (right). The deformity to be reduced was described as rotation around the rotation axis (middle). (B) The bone defect (arrowhead) was estimated, and the appropriate site and direction of the screw insertion (arrow) were determined by viewing the reduced scaphoid model on transparent mode from various angles.

els) of the bones (displaced nonunion in situ, mirror image of the normal scaphoid, and reduced nonunion model with simulated screw insertion) were made based on the computer data in all patients and used as guides during surgery (Fig 3). The hard models of the estimated bone defect also were made after the same method in three patients and were used as guides when shaping the bone graft. The hard models were made of epoxy resin with an accuracy of 0.01 mm (C-met Co. Ltd., Yokohama, Japan).

Surgery was done through an anterior approach. The capsule of the wrist was incised longitudinally to expose the palmar surface of the scaphoid, and the nonunion site was compared with the hard models (Fig 4A–B). The displaced distal and proximal fragments were reduced by extending the wrist to match the contour of the anterior surface of the nonunited scaphoid to the shape of the hard model in reduced position. The sclerotic bone of the nonunion site was resected to visible bleeding. A bicortical bone graft was obtained from the iliac crest and shaped to match the bone defect. With three patients, the hard model of the estimated bone defect was used as a reference during this procedure, taking into consideration the fact that the actual bone graft is

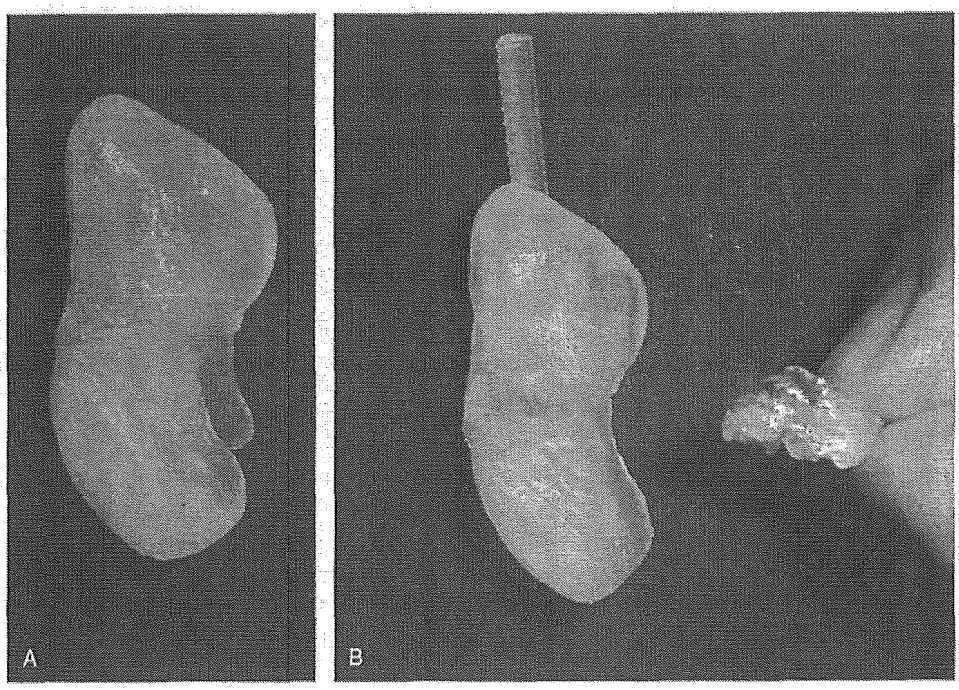

Fig 3A–B. Stereolithography of the scaphoid was made from computer data as shown in a (A) scaphoid nonunion model and a (B) reduced model with appropriate screw insertion and estimated bone defect.

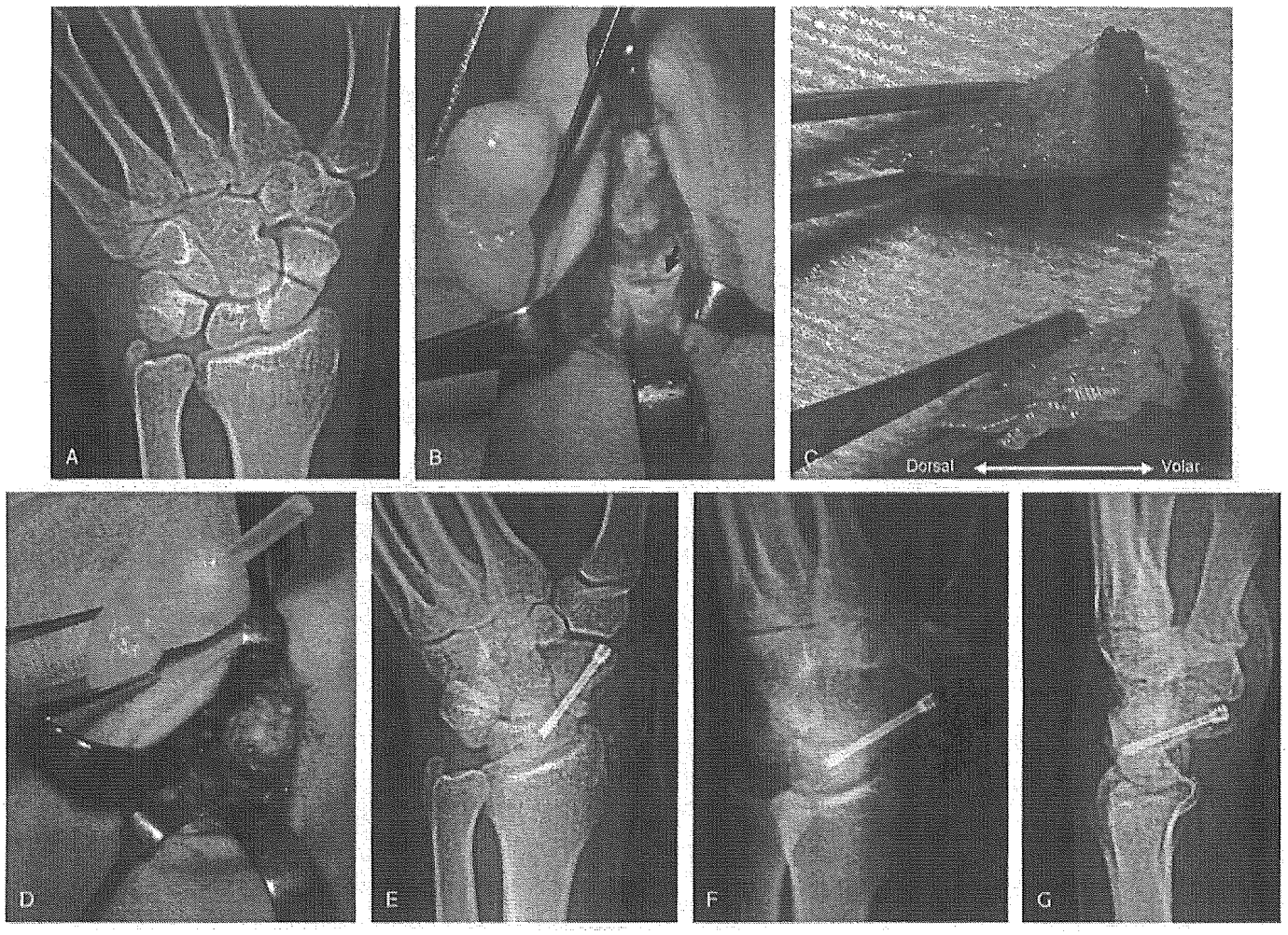

Fig 4A–G. (A) A plain radiograph shows scaphoid nonunion at the waist in Patient 7. (B) A nonunion site (arrow) was compared with the hard model. (C) The iliac bone graft was shaped using the hard model as a reference. (D) After inserting the bone graft, the site and direction of screw insertion were determined using the hard model as a guide. (E) The radiograph immediately after surgery shows good reduction of the displaced fragments and proper screw placement. (F) Anteroposterior and (G) lateral radiographs obtained 6 months after surgery show solid bone fusion with normal alignment.

larger than the estimated bone defect by the resected bone amount (Fig 4C). The graft was put into the bone defect followed by the insertion of a trial Kirschner wire (K wire) 0.8–1.2 mm in diameter to the simulated appropriate site and direction using the hard model as a guide (Fig 4D). After confirming position of the first K wire with an image intensifier, the second K wire was inserted alongside the first to prevent the scaphoid from loosening the reduction during the screw insertion. Subsequently, the first K wire was removed, and internal fixation was accomplished by placing a double-threaded screw in line with the removed K wire (Fig 4E). In patients in whom a cannulated screw was used, the screw was inserted through the first K wire. A Herbert screw (Zimmer Inc., Warsaw, IN) was used in four patients, a Scaphoid screw (Hit Medica Srl, Rimini, Italy) was used in two patients, and a DTJ screw (MEIRA Corp, Nagoya, Japan) was used in one patient. The latter two screws were cannulated variants of the double-threaded screw for small bones. The wrist was immobilized for 4 weeks postoperatively, and a short arm splint was applied until bone union was confirmed radiographically (Fig 4F–G).

To evaluate carpal alignment, the radiolunate angle (RLA), scapholunate angle (SLA), and capitolunate angle (CLA) of the plain radiographs for both wrists were measured before and after the surgery and at the most recent followup.[25] The standard deviation of the intraobserver and interobserver variations of these radiographic measurements has been reported as less than 3°.[23] Screw placement was considered appropriate when postsurgical radiographs showed its insertion along the longitudinal axis of the scaphoid into the center of the proximal fragment on the AP, lateral, and scaphoid views. Bone union was considered complete when the fracture line disappeared and the bone trabeculae continuity was confirmed on all three radiographic views.[10,31]

Clinical evaluation was done an average of 14.2 months (range, 12–16 months) after surgery, and 12 (range, 9–14 months) months after bone healing. To evaluate the clinical results, the rating system of Cooney et al[7] was used. Ratings were given to each patient as follows: pain, function status, range of motion (ROM) of the wrist, and grip strength measured by percentages of normal (range, 0–25 points). Points were accumulated for the four categories. A satisfactory result totaled 65 or more points. The clinical rating system is not a patient-generated system validated against independent measures, but has been widely used in its original or modified forms in major studies dealing with wrist problems.[2,8,17,18,34,35] Clinical ratings were made by two of the authors (TM, HM) who were the operating surgeons. Radiographic measures were made by one author (AG) who was blinded to the clinical results.

RESULTS

In all patients, normalized carpal alignment, appropriate screw placement, and solid bone fusion seen on radiographs were accomplished with satisfactory clinical results. The mean of SLA, RLA, and CLA were 69.4°, –6.0°, –3.8° before surgery and 49.1°, 2.8°, 3.9° after surgery, respectively (Table 2). The mean SLA, RLA, and CLA of the contralateral normal wrist were 49.9°, 5.0° and 8.6°, respectively. The radiographic parameters had not changed at the most recent followup. The screws were positioned appropriately in all patients as planned before surgery. On average, all patients obtained solid bone fusion by 9.6 weeks (range, 8–12 weeks) after surgery. Postoperative radiographs showed no progressive osteoarthritis. The postoperative wrist score ranged from 65–100 points (average, 89 points) (Table 3). The average flexion-extension ROM was 138° (range, 115°–160°), and the average radioulnar ROM was 64° (range, 50°–75°). Grip strength was 80–100% of the uninjured wrist with an average of 90%. One patient (Patient 4) had wrist pain on extension of the affected wrist and restricted extension ROM despite solid scaphoid union at the most recent followup. In this patient, an osteophyte at the dorsal ridge was evident on the 3-D model, although it was not evident on plain radiographs. The osteophyte was thought to be the cause of the fair result of this patient. The other patients reported neither wrist pain nor functional impairment at the most recent followup.

During the operation, stereolithography models were of great help and provided good surgical orientation. Using these hard models, we were able to reduce the nonunions and insert the screws according to the preoperative plan. Hard models of the bone defect were fabricated in three of the seven patients, and the models were useful in two patients. In the third patient, because intraoperative findings necessitated extensive resection of bone at the nonunion site, the hard model was smaller than the appropriate bone graft.

In the computer simulation, the distal fragment volarly rotated 34.8° (range, 18.7°–70.9°) relative to the proximal fragment around the rotation axis, which ran in a dorsoulnar to radiovolar direction penetrating the head of the capitate in all the patients (Fig 5). The mean volumes of the distal fragment, the proximal fragment, and the estimated bone defect were 1518 mm^3, 1346 mm^3 and 219 mm^3, respectively. The mean volume of the contralateral normal scaphoid was 3045 mm^3. The estimated bone defect was triangular, with a volar base and dorsal apex. The dimensions were 5.5 mm (range, 3.8–7.3 mm) in anterior thickness, 9.7 mm (range, 7.5–12.1 mm) in depth, and 10.7 mm (range, 9.1 to 12.8 mm) in width on average. The appropriate point of screw insertion was located 3 mm ulnar and dorsal to the center of the scaphoid tubercle. The estimated largest length of the screw was an average of 28.1 mm (range, 26–32 mm), and the length of the screw used in the actual surgery was an average of 24.3 mm (range, 22–28 mm).

DISCUSSION

Management of a displaced scaphoid nonunion is challenging. Solid bone fusion with normalized carpal align-

TABLE 2. Radiographic Evaluation

Patient Number	Time Until Bone Union (weeks)	SLA Preoperative/ Postoperative (unaffected side)	RLA Preoperative/ Postoperative (unaffected side)	CLA Preoperative/ Postoperative (unaffected side)
1	6	60/50 (45)	10/14 (17)	5/15 (17)
2	7	85/45 (50)	–17/–5 (–3)	–18/0 (3)
3	12	85/50 (45)	–12/–5 (–3)	–10/0 (2)
4	12	70/55 (60)	–13/0 (5)	0/5 (7)
5	10	65/45 (50)	0/10 (13)	–2/11 (15)
6	9	50/45 (46)	0/3 (5)	2/5 (10)
7	12	65/45 (48)	–5/0 (3)	–2/2 (3)

SLA = scapholunate angle; RLA = radioscaphoid angle; CLA = capitolunate angle

TABLE 3. Clinical Evaluation

Patient Number	Flexion/Extension Range (degrees) (F/E)	Radioulnar Range (degrees) (R/U)	Grip Strength (kg) (affected/unaffected)	Pain	Wrist Score
1	150 (80/70)	70 (20/50)	24/24	None	100
2	135 (70/65)	55 (15/40)	46/49	None	90
3	145 (75/70)	60 (20/40)	48/49	None	100
4	115 (70/45)	50 (15/35)	36/45	Mild	65
5	120 (60/60)	65 (25/40)	53/60	None	90
6	160 (80/80)	75 (25/50)	37/45	None	90
7	135 (60/75)	70 (20/50)	43/50	None	90

ment is the key to achieving good functional results.[1] The importance of anatomic reduction has been emphasized by numerous investigators.[9,13,30,34] Patients with malunited scaphoid fractures have a greater incidence of osteoarthritis and impaired wrist function than patients whose fractures unite anatomically.[2,14,25,33] Altered kinematics and intraarticular incongruity predispose the wrist to having progressive osteoarthritis develop. Tsuyuguchi et al[35] reported that substantially better functional results could be obtained in patients with normalized carpal alignment than in patients with persistent DISI deformity as seen by increased SLA after surgery. In a simulation study using cadavers, the loss of wrist extension was proportional to the angular deformity of the scaphoid, and complete loss of wrist extension occurred at 30° angulation.[5] Given these research findings, it is desirable to restore as much precise anatomic reduction as possible when treating scaphoid nonunion, although the rate of malunion after surgery has been reported to be 5.4–50%.[11,21,34,35] Fernandez[12,13] advocated the insertion of a wedge- or trapezoidal-shaped iliac bone graft of which the size was planned using preoperative radiographs through a volar approach. However, in preoperative planning based on plain radiographs, two-dimensional information does not always reliably correct carpal malalignment.[34] Concerning solid bone fusion after scaphoid nonunion surgery, appropriate screw insertion is of great importance. The optimum positioning of screw placement is difficult even under fluoroscopic control, and the rate of improper screw placement has been reported as 19–29%.[1,9] The high incidence is presumably because of the complicated 3-D configuration of the scaphoid bone.

Our approach to solving these problems was to simulate the surgery using 3-D models derived from CT data. Although 3-D CT models have been used to elucidate the pathomechanism of scaphoid nonunion,[4,6,19,27,29] the attempt to simulate the surgery for scaphoid nonunion with 3-D information has not been reported. Although the limitation of the current study includes small numbers of subjects, lack of concurrent controls, and a patient-generated validated means of outcome assessment, it is the first trial investigating the usefulness of 3-D computer simulation in this field.

In our method, the deformity could be measured three dimensionally. The amount of displacement of the distal fragment relative to the proximal fragment was expressed as rotation around a rotation axis and observed three dimensionally. Furthermore, we were able to know the estimated bone defect, the optimum site, and the direction of

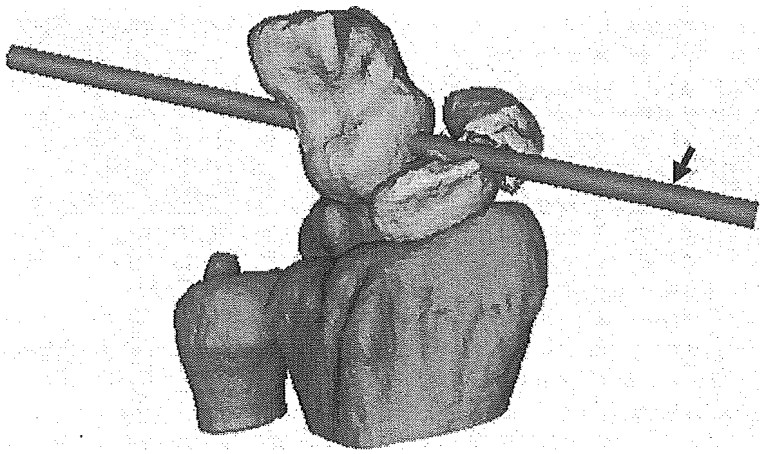

Fig 5. The rotation axis around which the distal fragment rotates runs in the dorsoulnar to radiovolar direction penetrating the head of the capitate (arrow) (Patient 3).

screw insertion. The estimated bone defect was consistently triangular, with its base facing volarly, and a width of 4–7 mm. A full-sized plastic model made by stereolithography was used to reflect the results of preoperative simulation in the actual surgery. This proved useful for acquisition of intraoperative orientation, reduction of the displaced nonunion, shaping of the bone graft, and appropriately positioned screw insertion. Radiographic results of all seven patients showed normal carpal alignment and optimal screw placement. Clinical results were either excellent or good, with the exception of one patient who had minor osteoarthritic changes seen on 3-D images but not seen on plain radiographs. These results are encouraging when compared with the previously reported incidence of malunion and improper screw placement after surgery.[1,9,11,21,34,35]

The scaphoid models we used on the computer were of only surface shells, with no internal information such as bony sclerosis, osteoporosis, or cyst formation. Although surface models are easy to handle on a computer program, they do not provide adequate information regarding the amount of sclerotic bone to be resected during computer simulation. We used hard models of the estimated bone defect as guides for shaping the bone graft in three patients. These models proved useful in two patients in whom sclerotic changes were not severe. It was not useful in one patient because of the large amount of sclerotic bone that needed resecting. The size of the actual bone graft should be determined by adding the resected amount to the estimated bone defect. This point will require improvement in the future. The other shortcoming of our method is the need for CT scanning, analysis of CT data, and hard model development. Currently, the process requires 10 minutes for CT data acquisition, 2 hours of an operator's time, and 1 hour for hard model development. It is likely that these problems will be eliminated with the advancement of computer technology.

Three-dimensional computer simulations were found to be useful in achieving accurate correction of scaphoid nonunions, and for maintaining normal carpal alignment to yield a good clinical outcome.

Acknowledgments

We thank A/Prof. Yoshinobu Sato, from the Department of Medical Robotics and Image Sciences, in helping to develop the computer program. We also thank Dr. Koji Yamamoto and Dr. Kakukro Denno for clinical contributions, and Mr. Ryoji Nakao for assistance in software management.

References

1. Adams BD, Blair WF, Reagan DS, Grundberg AB: Technical factors related to Herbert screw fixation. J Hand Surg 13A:893–899, 1988.
2. Amadio PC, Berquist TH, Smith DK, et al: Scaphoid malunion. J Hand Surg 14A:679–687, 1989.
3. Audette MA, Ferrie FP, Peters TM: An algorithmic overview of surface registration techniques for medical imaging. Med Image Anal 4:201–217, 2000.
4. Belsole RJ, Hilbelink DR, Llewellyn JA, et al: Computed analyses of the pathomechanics of scaphoid waist nonunions. J Hand Surg 16A:899–906, 1991.
5. Burgess RC: The effect of simulated scaphoid malunion on wrist motion. J Hand Surg 12A:774–776, 1987.
6. Compson JP: The anatomy of acute scaphoid fractures: A three-dimensional analysis of patterns. J Bone Joint Surg 80B:218–224, 1998.
7. Cooney WP, Bussey R, Dobyns JH, Linscheid RL: Difficult wrist fractures: Perilunate fracture-dislocations of the wrist. Clin Orthop 214:136–147, 1987.
8. Cooney WP, Linscheid RL, Dobyns JH: Triangular fibrocartilage tears. J Hand Surg 19A:143–154, 1994.
9. Cooney WP, Linscheid RL, Dobyns JH, Wood MB: Scaphoid nonunion: Role of anterior interpositional bone grafts. J Hand Surg 13A:635–650, 1988.
10. Daly K, Gill P, Magnussen PA, Simonis PB: Established nonunion of the scaphoid treated by volar wedge grafting and Herbert screw fixation. J Bone Joint Surg 78B:530–534, 1996.
11. Eggli S, Fernandez DL: Unstable scaphoid fracture nonunion: A medium-term study of anterior wedge grafting procedures. J Hand Surg 27B:36–41, 2002.
12. Fernandez DL: A technique for anterior wedge-shaped grafts for scaphoid nonunions with carpal instability. J Hand Surg 9A:733–737, 1984.
13. Fernandez DL: Anterior bone grafting and conventional lag screw fixation to treat scaphoid nonunions. J Hand Surg 15A:140–147, 1990.
14. Fernandez DL, Eggli S: Scaphoid nonunion and malunion. Hand Clin 17:631–646, 2001.
15. Fisk GR: Carpal instability and the fractured scaphoid. Ann R Surg Engl 46:63–76, 1970.
16. Handels H, Ehrhardt J, Plotz W, Poppl SJ: Virtual planning of hip operations and individual adaption of endoprostheses in orthopaedic surgery. Int J Med Inf 58:21–28, 2000.
17. Harley BJ, Werner FW, Boles SD, Palmer AK: Arthroscopic resection of arthrosis of the proximal hamate: A clinical and biomechanical study. J Hand Surg 29A:661–667, 2004.
18. Herrera M, Chapman CB, Roh M, et al: Treatment of unstable distal radius fractures with cancellous allograft and external fixation. J Hand Surg 24A:1269–1278, 1999.
19. Hidaka Y, Nakamura R: Progressive patterns of degenerative arthritis in scaphoid nonunion demonstrated by three-dimensional computed tomography. J Hand Surg 23B:765–770, 1998.
20. Inoue G, Sakuma M: The natural history of scaphoid non-union: Radiographical and clinical analysis in 102 cases. Arch Orthop Trauma Surg 115:1–4, 1996.
21. Jiraneck WA, Ruby LK, Millender LB, et al: Long-term results after Russe bone-grafting: The effect of malunion of the scaphoid. J Bone Joint Surg 74A:1217–1227, 1995.
22. Kinzel GL, Hall AS, Hillberry BM: Measurement of the total motion between two body segments: I. Analytic development. J Biomech 5:93–105, 1972.
23. Larsen CF, Stigsby B, Lindequist S, et al: Observer variability in measurements of carpal bone angles on lateral wrist radiographs. J Hand Surg 16A:893–898, 1991.
24. Lorensen WP, Cline HE: Marching cubes: A high resolution 3D surface construction algorithm. Comput Graph (ACM) 21:163–169, 1987.
25. Lynch NM, Linscheid RL: Corrective osteotomy for scaphoid malunion: Technique and long-term follow-up evaluation. J Hand Surg 22A:35–43, 1997.
26. Mack GR, Bosse MJ, Gelberman RH, Yu E: The natural history of scaphoid non-union. J Bone Joint Surg 66A:504–509, 1984.

27. Moritomo H, Viegas SF, Elder KW, et al: Scaphoid nonunions: A 3-dimensional analysis of patterns of deformity. J Hand Surg 25A:520–528, 2000.
28. Nakamura R, Hori M, Horii E, Miura T: Reduction of the scaphoid fracture with DISI alignment. J Hand Surg 12A:1000–1005, 1987.
29. Nakamura R, Imaeda T, Horii E, et al: Analysis of scaphoid fractures displacement by three-dimensional computed tomography. J Hand Surg 16A:485–492, 1991.
30. Nakamura R, Imaeda T, Miura T: Scaphoid malunion. J Bone Joint Surg 73B:134–137, 1991.
31. Rajagoplan BM, Squire DS, Samuels LO: Results of Herbert-screw fixation with bone-grafting for the treatment of nonunion of the scaphoid. J Bone Joint Surg 81A:48–52, 1999.
32. Smith DK, Cooney WP, An KN, et al: The effect of simulated unstable scaphoid fractures on carpal motion. J Hand Surg 14A:283–291, 1989.
33. Stehlik J, Bartos M, Kestranek Z, et al: Application of numerical modeling of osteotomy to orthopaedic practice. Int J Med Inf 45:75–82, 1997.
34. Tomanio MM, King J, Pizillo M: Correction of lunate malalignment when bone grafting scaphoid nonunion with humpback deformity: Rationale and results of a technique revisited. J Hand Surg 25A:322–329, 2000.
35. Tsuyuguchi Y, Murase T, Hidaka N, et al: Anterior wedge-shaped bone graft for old scaphoid fractures or non-unions: An analysis of relevant carpal alignment. J Hand Surg 20B:194–200, 1995.
36. Vender MI, Watson HK, Wiener BD, Black DM: Degenerative change in symptomatic scaphoid nonunion. J Hand Surg 12A:514–519, 1987.